Evaluating the Evidence for Neuroimaging-Based Biotypes of Psychiatric Vulnerability in the Acute Aftermath of Trauma

Online Supplement

Supplementary Methods

Clinical Assessments. The PTSD Checklist for DSM-IV (PCL-IV)[1] measures the distress caused by each clinical symptom over the past month, using a 5-point scale ranging from 1 (not at all) to 5 (extremely distressing). At each time-point, PCL item scores were summed to yield a secondary continuous measure of PTSD symptom severity, in addition to CAPS total scores. The PCL was shown to have high test-retest reliability over a three-day period (r = 0.96) and very high internal consistency (α = 0.97), as well as a high correlation with CAPS[2]. The Beck Anxiety Inventory (BAI)[3] measures common symptoms of anxiety over the past week using individual item scores ranging from 0 (not al all) to 3 (severely). It was shown to discriminate anxious diagnostic groups (panic disorder, generalized anxiety disorder, etc.) from non-anxious diagnostic groups (major depression, dysthymic disorder, etc.), and was moderately correlated with other anxiety rating scales[4]. At each time-point, BAI item scores were summed to yield a continuous measure of anxiety symptom severity.

functional MRI (fMRI) Tasks. *Threat Reactivity Task.* To probe participants' reactivity to social threat cues, we used the well-known Hariri's face-matching task[5]. In this paradigm, participants were instructed to select the face (located at the bottom right or bottom left of the screen) that matches the target face (located at the top of the screen), as accurately and as quickly as possible. The task included four blocks of shapes, and four blocks of emotional faces (angry, fearful, surprised, and neutral faces). The order of the emotional faces blocks was counterbalanced between subjects, as well as within-subjects across different time-points, using four different orders for this task.

Reward Reactivity fMRI Task. To probe participants' reward reactivity, we used an interactive naturalistic gambling game, termed the 'Safe or Risky Domino Choice' (SRDC) task. The effectiveness of the SRDC to detect individuals' sensitivity to risk, punishment, and reward was previously validated in both healthy and clinical populations[6–11]. In this task, individuals played a 2-player competitive game, in which they were required to make risky choices to win. While participants were told that the opponent is the experimenter and that their choices can increase their chances of winning, the computer randomly generated the opponent's responses in a predetermined pattern to allow a balanced design (exposing the player's choices 50% of the time). Each round of the game is composed of four intervals. First, the player chooses which chip to play next, either a matching choice (e.g., a chip with at least one of the master chip's numbers) or a non-matching choice. Next, they move the cursor to the chosen chip and place it

facing down adjacent to the master chip. Participants then wait for the opponent's response to see whether he/she challenges their choice by uncovering the chosen chip or not. Players' choices and opponents' responses are interactively determined by the flow of the game round after round, creating a natural progression of a game situation that lasts 4 minutes or until the player wins the game by disposing of all his/her chips. Each player played consecutively for 14 minutes (approximately 3–4 game rounds). The focus of this work was on the neural responses to different outcomes, specifically while receiving rewards vs. when receiving punishments. For more details, see Fig. 1 in Ben-Zion et al. (2021)[12] and its supplementary methods.

fMRI Data Preprocessing. Raw DICOM data images were converted to NIFTI format and organized to conform to the 'Brain Imaging Data Structure' specifications (BIDS)[13]. Quality control steps of both the anatomical and functional data were conducted using: (1) Visual inspection for conversion errors and data exclusion criteria (e.g., anatomical abnormalities, signal drop-out); (2) MRI Quality Control (MRIQC)[14] tool developed by the Poldrack Lab at Stanford University for the use at the Center for Reproducible Neuroscience (CRN). Preprocessing was conducted using fMRIPrep version 1.5.8[15], a Nipype based tool[16], and included:

(1) Preprocessing of the anatomical data. Within the fMRIPrep framework, T1-weighted (T1w) images were corrected for intensity non-uniformity (INU) using `N4BiasFieldCorrection'[17] version 2.1.0, distributed with `AntsApplyTransforms` (ANTs) version 2.2.0. The T1w-reference was then skull-stripped with a Nipype implementation of the `antsBrainExtraction.sh` workflow (ANTs version 2.2.0), using OASIS30-ANTs as a target template. A T1w-reference map was computed after registration of the INU-corrected T1w images using `mri_robust_template` (FreeSurfer version 6.0.1). Volume-based spatial normalization to the ICBM 152 Nonlinear Asymmetrical template version 2009c ('MNI152NLin2009cAsym')[18] was performed through nonlinear registration with `antsRegistration` tool (ANTs version 2.2.0), using brain-extracted versions of both T1w volume and template. Brain tissue segmentation of cerebrospinal fluid (CSF), white matter (WM), and gray matter (GM) were performed on the brain-extracted T1w images using FMRIB's Automated Segmentation Tool ('FAST'), as part of FSL version 5.0.9 [19].

(2) Preprocessing of the functional data. For each of the BOLD runs found per subject (across all tasks and sessions), the following preprocessing was performed. First, a reference volume and its skull-stripped version were generated using a custom methodology of fMRIPrep. Susceptibility distortion correction (SDC) was omitted. The BOLD reference was then co-registered to the T1w reference using 'bbregister' (FreeSurfer) which implements boundary-

based registration[20]. Co-registration was configured with 9 degrees of freedom to account for distortions remaining in the BOLD reference. Head-motion parameters with respect to the BOLD reference (transformation matrices, and six corresponding rotation and translation parameters) were estimated before any spatiotemporal filtering using `mcflirt` (FSL version 5.0.9)[21]. BOLD runs were slice-time corrected using `3dTshift` from AFNI version 16.2.07. The BOLD time-series (including slice-timing correction) were resampled onto their original, native space by applying the transforms to correct for head-motion. These resampled BOLD time-series will be referred to as 'preprocessed BOLD in original space', or just 'preprocessed BOLD'. First, a reference volume and its skull-stripped version were generated using a custom methodology of fMRIPrep. Several confounding time-series were calculated based on the preprocessed BOLD: framewise displacement (FD), DVARS, and three region-wise global signals (extracted within the CSF, WM, and whole-brain masks). Additionally, a set of physiological regressors were extracted to allow for component-based noise correction ('CompCor')[22]. Principal components were estimated after high-pass filtering of the pre-processed BOLD time-series (using a discrete cosine filter with 128s cut-off) for the two 'CompCor' variants: temporal ('tCompCor') and anatomical ('aCompCor'). Six 'tCompCor' components were then calculated including only the top 5% variable voxels within that subcortical mask. For aCompCor, six components were calculated within the intersection of the subcortical mask and the union of CSF and WM masks calculated in T1w space, after their projection to the native space of each functional run. For each CompCor decomposition, the k components with the largest singular values were retained, sufficient to explain 50% of the variance across the nuisance mask. The remaining components were dropped from consideration. The head-motion estimates calculated in the correction step were also placed within the corresponding confounds file. The confound time series derived from head motion estimates and global signals were expanded with the inclusion of temporal derivatives and quadratic terms. Frames that exceeded a threshold of 0.5mm FD or 1.5 standardized DVARS were annotated as motion outliers. All re-samplings were performed with a single interpolation step by composing all the pertinent transformations. Gridded (volumetric) re-samplings were performed using 'antsApplyTransforms' (ANTs), configured with Lanczos interpolation to minimize the smoothing effects of other kernels[23]. Non-gridded (surface) re-samplings were performed using `mri_vol2surf` (FreeSurfer). Many internal operations of FMRIPREP use `Nilearn` version 0.6.2[24], mostly within the BOLD-processing workflow. Finally, spatial smoothing was performed with an isotropic Gaussian kernel of 6mm FWHM (full-width at half-maximum).

fMRI Data Analysis. Analysis of the functional data of both fMRI tasks was performed using Statistical Parametric Mapping (SPM)[25] version 12 (SPM-12). For the threat reactivity task, blocks of fearful and neutral stimuli were modeled separately using the onset and duration time of each block, convolved with a canonical hemodynamic response function. The neural contrast of watching fearful faces vs. watching neural faces (i.e., Fearful > Neutral) was used for the region-of-interest (ROI) extraction. For the reward reactivity task, neural responses to outcomes of rewards and punishments were as separate experimental conditions in an event-related design. A "false" condition was modeled including trials in which participants had no actual choice (i.e., when only matching or only non-matching chips remained to choose from), and when they did not respond within the defined time (i.e., within 10 seconds after the "go" signal). to choose a chip (during 10 seconds starting with the "go" signal). Movement events were modeled when players had to move and choose a chip (during both "ready" and "go" intervals). The implicit baseline was defined as both decision-making intervals ("choose") and false rounds ("false"). The neural contrast of receiving both rewarding outcomes versus receiving both punishing outcomes, (i.e., Rewards > Punishments) was used for the ROI extraction. In all first-level models, white matter, CSF and global signal time courses were included as nuisance regressors. The full details of the analysis of the threat and reward tasks reactivity task can be found in Ben-Zion et al. (2020)[26] and Ben-Zion et al. (2021)[12], respectively.

Participants' mean activations (average beta weights) across all voxels in each region-of-interest (ROI) were extracted from individuals' first-level contrasts using the MarsBaR toolbox[27]. In line with Stevens et al.[28], all ROIs were defined bilaterally using anatomical boundaries. For the threat reactivity task, ROIs included the amygdala[29], insula[30], subgenual anterior cingulate cortex (sgACC) and dorsolateral anterior cingulate cortex (dACC) as defined by Brodmann Areas 25 and 32, respectively. For the reward reactivity task, ROIs included the nucleus accumbens (NAcc)[31], orbitofrontal cortex (OFC)[32] and amygdala[29]. Similar to the original article, we did not require that all ROIs show significant task-related activation, as some regions with high inter-individual variability may not be significantly activated in group-level analyses[28]. Like Stevens et al., fMRI data from each ROI were z-scored to minimize range effects (prior to clustering). Outliers were further replaced with a cap score at M±3SD.

Clustering Analysis. In more details, we first obtained the covariance matrix of the fMRI tasks and ROIs used for the clustering analysis (7 features). Second, we simulated n=1999 random samples with the size of our original dataset (n=130) from this covariance matrix assuming the variables to be multivariate and normally distributed. Third, we ran the same hierarchical

clustering procedure (as performed on the real data) on each random sample and calculated the best obtained Hartigan's distance metric and Silhouette width metric. Thereby, we obtained an empirical null distribution of these two distance metrics. The p-value was then defined as the ranks of the indices values in the null distribution smaller than the value of the indices observed in the original data.

Supplemental Results

Participants' Demographic and Clinical Characteristics. Chi-square tests (categorical variables) and independent t-tests (continuous variables) were used to assess the differences in participants' demographic and clinical characteristics between this study (n=130; see Table 1 in the main text) and the original one[28] (discovery: n=69, replication: n=77; see Table 1 in Stevens et al.[28]). First, there was no significant difference in age between this study's participants to those in the discovery (t=1.754, p=0.081) or replication (t=0.747, p=0.456) cohorts of the original study. Second, there was a significant difference in gender between this study's sample and the discovery cohort of Stevens et al. (χ^2=12.629, p<0.001), which included more females (74%) compared to our cohort (48%). Nevertheless, there was no significant difference in gender between this study's participants to those in the replication cohort of Stevens et al. (χ^2=3.598, p=0.058). Third, there was a significant difference in trauma type between our cohort and both discovery (χ^2=7.035, p=0.008) and replication (χ^2=30.428, p<0.001) cohorts of the original work. While the discovery cohort had more MVA survivors (69 out of 69, 100%) than the sample in this work (115 out of 130, 88%), the replication cohort had significantly fewer MVA survivors (41 out of 77, 53%). Finally, participants in this report had an average of 14.25±2.74 education years, with a 95% confidence interval (CI) ranging from 13.76 to 14.75 years. This is comparable to the qualitative description of education level in both cohorts of Stevens et al., where the majority of individuals were between 'High-school diploma/GED' to a bachelor's degree (discovery: 63 out of 69, 91%; replication: 63 out of 77, 83%). We were not able to find in the original study information to compare participants' marital status or severity of PTSD and anxiety. Furthermore, this dataset did not include, hence could not compare, other demographic characteristics that were reported in Stevens et al.'s work: race/ethnicity, employment status, yearly family income, and childhood maltreatment assessment. Finally, it is possible that the clusters in both studies reflect other pre-trauma factors that were not measured, such as genetic markers, family history, or temperament[33].

Whole-brain Activations during Reward Reactivity Task. While the two studies used different fMRI tasks to probe reward reactivity (SRDC paradigm[12] versus Delgado's monetary reward task[34]), whole-brain neural activations seem to be qualitatively similar. Brain images showing task-responsive voxels across all participants in the original work for the contrast of Monetary Gains > Losses (Fig. 1D in Stevens et al., 2021[28]) overlap with those found for all participants in this work for the contrast of Rewards > Punishments in our work (Fig. S1 in Ben-

Zion et al., 2021[12]), with the most significant positive activations in reward areas (NAcc / Ventral Striatum).

Clustering of Individuals Using Task-based fMRI at One-Month Posttrauma. To avoid redundancy, and in line with Stevens et al.[28], we reported the 4-cluster solution in the main text and the 2-cluster solution here in the supplemental results.

Assessment of the different fMRI activation patterns at one-month posttrauma among the two-cluster solution revealed a subgroup of 18 individuals showing high reactivity of all the brain regions to threat and rewards (Cluster 2 in Fig. S2.b). Examining the clustering tree (Fig. S2.a), we a subgroup (Cluster 2, n=18) which is identical to Cluster 4 in the four-cluster solution (see Fig. 2b). The other large group (Cluster 1, n=112) showed average activation across brain regions to threat and rewards (contrast estimates~0). This cluster includes all three subgroups found in the four-cluster solution together (Clusters 1-3 in Fig. 2c).

The assignment for the two clusters was unrelated to any of the demographic characteristics (participant's age, gender, or marital status; for all: p>0.05).

Finally, the 2-cluster solution showed the optimal Silhouette width index. Using a simulation approach aiming to test the significance of the clusters[34,35], we found that this index was statistically significant (Silhouette width index=0.240, p=0.005; Fig. S1.c). In other words, it is unusual to observe such an index when the hierarchical clustering is performed on a multivariate normally distributed dataset (with no clusters), supporting the fact that two clusters (as shown in Fig. S2) were more likely than no clusters at all.

Figure S1. Optimal Number of Clusters and Clustering Significance. a. Weighted sum of squares for within-cluster point distances across a range of cluster solutions (from k=1 to k=6 clusters). The optimal solution according to Hartigan's distance index is denoted with a dotted line. **b.** Silhouette width for a range of cluster solutions after hierarchical clustering using Wilk's criterion. Width summarizes the distance of points within a cluster relative to points outside the cluster. The dotted line indicates maximum silhouette width, representing the optimal solution. **c.** The null distribution of Hartigan's distance index. Although this index is maximized at k=4 clusters, these results are not unusual even for the data simulated from a Gaussian distribution with no clusters. Those criteria do not imply evidence for the existence of clusters in our data.

d. The null distribution of Silhouette width index. Results are unusual compared to data simulated from a Gaussian distribution with no clusters, providing evidence for the existence of this 2-cluster solution in our data.

Figure S2. fMRI Profiles of the Two Clusters among Trauma Survivors (n=130). a. Dendrogram illustrates the two-cluster solution (different colors). **b.** Cluster differences (mean and SD) for standardized contrast estimates extracted from the ROIs across the threat (fearful > neutral faces) and reward (rewards > punishments) contrasts. T=Threat, R=Reward, Amy=Amygdala
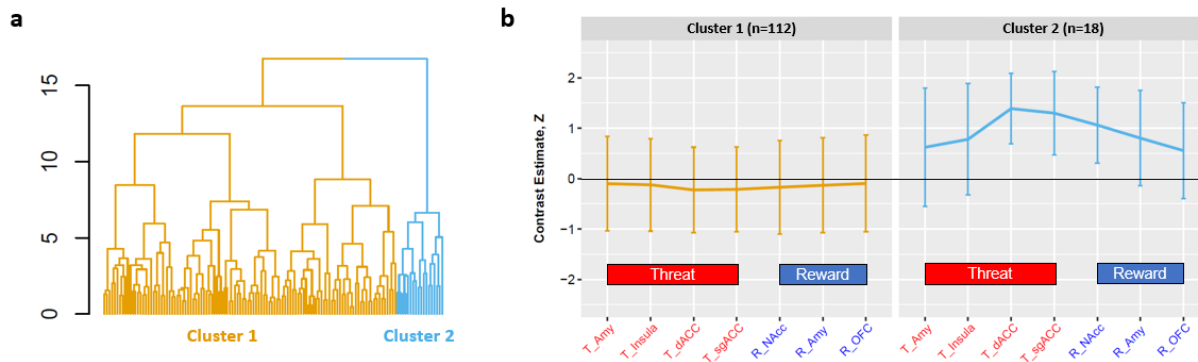
Figure S3. PTSD and Anxiety at 14-months Posttrauma among the Two Clusters of Trauma Survivors. Boxplots presenting the four clusters created based on neuroimaging data at 1-month posttrauma and their future clinical symptoms at 14-months posttrauma: CAPS-4 total scores (**a**), CAPS-5 total scores (**b**), PCL total scores (**c**), BAI total scores (**d**).

T3 = 14-months following ED admission.
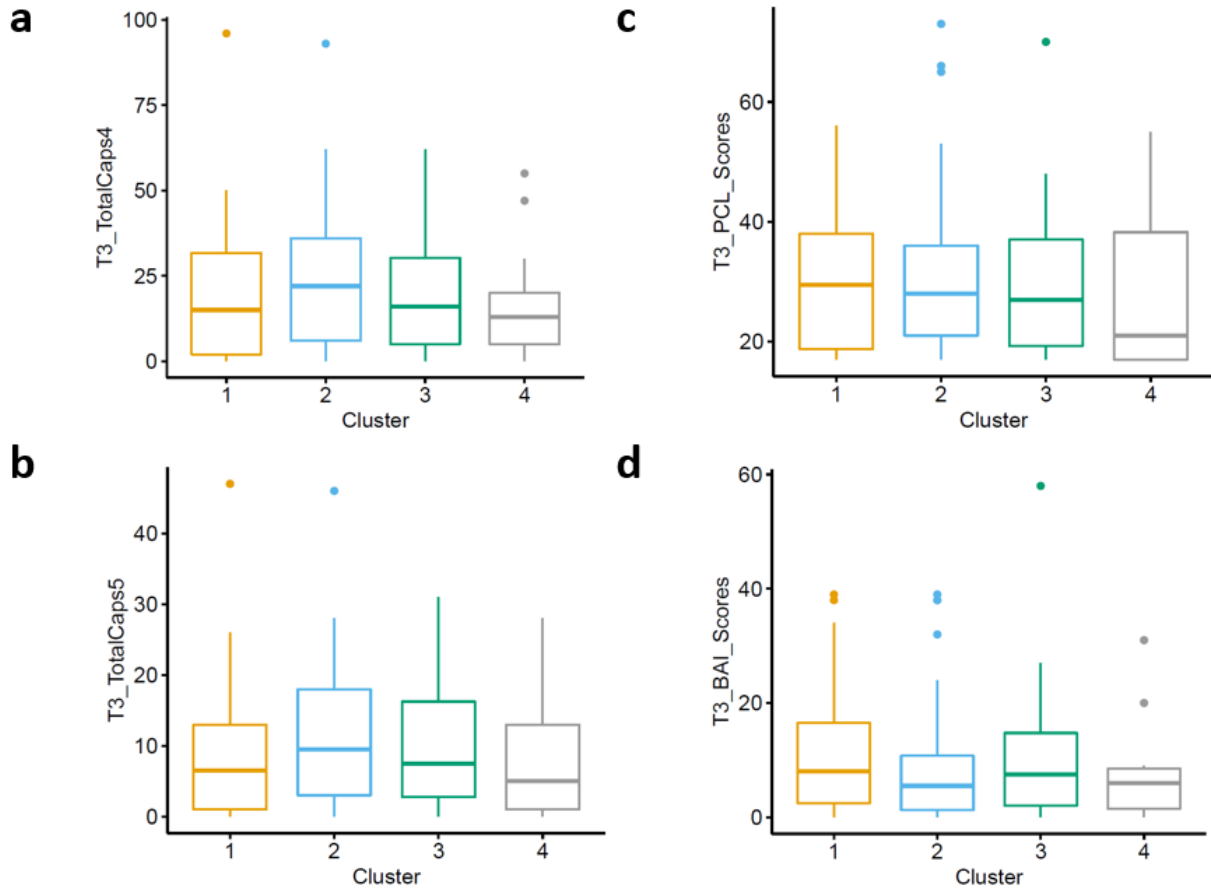
Supplemental References

1.   Weathers, F.W. Litz, B. T., Herman, D. S., Huska, J. A., & Keane TM. The PTSD Checklist: Reliability, Validity, and Diagnostic Utility. *Annual Meeting of the International Society for Traumatic Stress Studies San Antonio, TX*. Published online 1993.

2.   Blanchard EB, Jones-Alexander J, Buckley TC, Forneris CA. Psychometric properties of the PTSD checklist (PCL). *Behaviour Research and Therapy*. 1996;34(8):669-673. doi:10.1016/0005-7967(96)00033-2

3.   Beck A, Epstein N, Brown G, Steer RA. An inventory for measuring clinical anxiety: Psychometric properties. *Journal of consulting and Clinical Psychology*. 1988;56(6):893.

4.   Fydrich T, Dowdall D, Chambless DL. Reliability and validity of the beck anxiety inventory. *Journal of Anxiety Disorders*. 1992;6(1):55-61. doi:10.1016/0887-6185(92)90026-4

5.   Hariri AR, Bookheimer SY, Mazziotta JC. Modulating emotional responses. *NeuroReport*. 2003;11(1):43-48. doi:10.1097/00001756-200001170-00009

6.   Kahn I, Yeshurun Y, Rotshtein P, Fried I, Ben-Bashat D, Hendler T. The role of the amygdala in signaling prospective outcome of choice. *Neuron*. 2002;33(6):983-994.

7.   Admon R, Lubin G, Rosenblatt JD, et al. Imbalanced neural responsivity to risk and reward indicates stress vulnerability in humans. *Cerebral Cortex*. 2013;23(1):28-35. doi:10.1093/cercor/bhr369

8.   Assaf M, Kahn I, Pearlson GD, et al. Brain activity dissociates mentalization from motivation during an interpersonal competitive game. *Brain Imaging and Behavior*. 2009;3(1):24-37. doi:10.1007/s11682-008-9047-y

9.   Thaler A, Gonen T, Mirelman A, et al. Altered reward-related neural responses in non-manifesting carriers of the Parkinson disease related LRRK2 mutation. *Brain Imaging and Behavior*. 2019;13(4):1009-1020. doi:10.1007/s11682-018-9920-2

10.   Hyatt CJ, Assaf M, Muska CE, et al. Reward-related dorsal striatal activity differences between former and current cocaine dependent individuals during an interactive competitive game. *PLoS ONE*. 2012;7(5):1-15. doi:10.1371/journal.pone.0034917

11.   Gonen T, Admon R, Podlipsky I, Hendler T. From animal model to human brain networking: Dynamic causal modeling of motivational systems. *Journal of Neuroscience*. 2012;32(21):7218-7224. doi:10.1523/JNEUROSCI.6188-11.2012

12.   Ben-Zion Z, Shany O, Admon R, et al. Neural Responsivity to Reward Versus Punishment Shortly After Trauma Predicts Long-Term Development of Posttraumatic

Stress Symptoms. *Biological Psychiatry: Cognitive Neuroscience and Neuroimaging*. 2022;7(2):150-161. doi:10.1016/j.bpsc.2021.09.001

13. Gorgolewski KJ, Auer T, Calhoun VD, et al. The brain imaging data structure, a format for organizing and describing outputs of neuroimaging experiments. *Scientific Data*. 2016;3. doi:10.1038/sdata.2016.44

14. Esteban O, Birman D, Schaer M, Koyejo OO, Poldrack RA, Gorgolewski KJ. MRIQC: Advancing the automatic prediction of image quality in MRI from unseen sites. *PLOS ONE*. 2017;12(9):e0184661. doi:10.1371/JOURNAL.PONE.0184661

15. Esteban O, Markiewicz CJ, Blair RW, et al. fMRIPrep: a robust preprocessing pipeline for functional MRI. *Nature Methods*. 2019;16(1):111-116. doi:10.1038/s41592-018-0235-4

16. Gorgolewski K, Burns CD, Madison C, et al. Nipype: A flexible, lightweight and extensible neuroimaging data processing framework in Python. *Frontiers in Neuroinformatics*. 2011;5. doi:10.3389/fninf.2011.00013

17. Tustison NJ, Avants BB, Cook PA, et al. N4ITK: improved N3 bias correction. *IEEE Trans Med Imaging*. 2010;29(6):1310-1320. doi:10.1109/TMI.2010.2046908

18. Fonov V, Evans A, McKinstry R, Almli C, Collins D. Unbiased nonlinear average age-appropriate brain templates from birth to adulthood. *Neuroimage*. 2009;Supplement 1(47):S102. doi:10.1016/S1053-8119(09)70884-5

19. Zhang Y, Brady M, Smith S. Segmentation of brain MR images through a hidden Markov random field model and the expectation-maximization algorithm. *IEEE Trans Med Imaging*. 2001;20(1):45-57. doi:10.1109/42.906424

20. Greve DN, Fischl B. Accurate and robust brain image alignment using boundary-based registration. *Neuroimage*. 2009;48(1):63-72. doi:10.1016/J.NEUROIMAGE.2009.06.060

21. Jenkinson M, Bannister P, Brady M, Smith S. Improved optimization for the robust and accurate linear registration and motion correction of brain images. *Neuroimage*. 2002;17(2):825-841. doi:10.1016/S1053-8119(02)91132-8

22. Behzadi Y, Restom K, Liau J, Liu TT. A component based noise correction method (CompCor) for BOLD and perfusion based fMRI. *Neuroimage*. 2007;37(1):90-101. doi:10.1016/J.NEUROIMAGE.2007.04.042

23. Lanczos C. Evaluation of Noisy Data. *http://dx.doi.org/101137/0701007*. 2006;1(1):76-85. doi:10.1137/0701007

24. Abraham A, Pedregosa F, Eickenberg M, et al. Machine learning for neuroimaging with scikit-learn. *Frontiers in Neuroinformatics*. 2014;8(FEB):14. doi:10.3389/FNINF.2014.00014/BIBTEX

25. Friston KJ, Ashburner JT, Kiebel SJ, Nichols TE, Penny WD. *Statistical Parametric Mapping: The Analysis of Functional Brain Images*. Vol 8.; 2007. doi:10.1016/B978-0-12-372560-8.50052-8

26. Ben-Zion Z, Zeevi Y, Keynan NJ, et al. Multi-domain potential biomarkers for post-traumatic stress disorder (PTSD) severity in recent trauma survivors. *Translational Psychiatry*. Published online 2020. doi:10.1038/s41398-020-00898-z

27. Brett M, Anton JL, Valabregue R, Poline JB. Region of interest analysis using an SPM toolbox. *Neuroimage*. Published online 2002.

28. Stevens JS, Harnett NG, Lebois LAM, et al. Brain-Based Biotypes of Psychiatric Vulnerability in the Acute Aftermath of Trauma. *American Journal of Psychiatry*. 2021;178(11):1037-1049. doi:10.1176/appi.ajp.2021.20101526

29. Tyszka JM, Pauli WM. In vivo delineation of subdivisions of the human amygdaloid complex in a high-resolution group template. *Hum Brain Mapp*. 2016;37(11):3979-3998. doi:10.1002/HBM.23289

30. Tzourio-Mazoyer N, Landeau B, Papathanassiou D, et al. Automated anatomical labeling of activations in SPM using a macroscopic anatomical parcellation of the MNI MRI single-subject brain. *Neuroimage*. 2002;15(1):273-289. doi:10.1006/NIMG.2001.0978

31. Pauli WM, Nili AN, Michael Tyszka J. Data Descriptor: A high-resolution probabilistic in vivo atlas of human subcortical brain nuclei. *Scientific Data*. 2018;5. doi:10.1038/sdata.2018.63

32. Fischl B, van der Kouwe A, Destrieux C, et al. Automatically parcellating the human cerebral cortex. *Cereb Cortex*. 2004;14(1):11-22. doi:10.1093/CERCOR/BHG087

33. Ioannidis K, Askelund AD, Kievit RA, van Harmelen AL. The complex neurobiology of resilient functioning after childhood maltreatment. *BMC Medicine*. 2020;18(1):1-16. doi:10.1186/S12916-020-1490-7/FIGURES/3

34. Speer ME, Bhanji JP, Delgado MR. Savoring the past: Positive memories evoke value representations in the striatum. *Neuron*. 2014;84(4):847-856. doi:10.1016/j.neuron.2014.09.028